J. Fluid Mech. (1988), *vol.* 191, *pp.* 177–195
Printed in Great Britain

Local effects of large-scale eddies on bursting in a concave boundary layer

By ROBERT S. BARLOW AND JAMES P. JOHNSTON†
Combustion Research Facility, Sandia National Laboratories, Livermore, CA 94550, USA

(Received 12 March 1987 and in revised form 17 October 1987)

Concave curvature has a destabilizing effect on a turbulent boundary layer that causes the formation of large-scale inflow and outflow regions. These structures are larger and more energetic than large eddies in a flat boundary layer, particularly in terms of velocity fluctuations normal to the wall. Flow visualization has suggested that the large-scale inflows and outflows have a strong influence on turbulence structure in the near-wall region. However, near-wall profiles of Reynolds-averaged quantities in the concave boundary layer do not indicate major structural changes. In this paper, the effects of concave curvature on near-wall structure are investigated in two flow cases: (i) the natural concave boundary layer, where the large-scale eddies do not have preferred spanwise locations and the layer remains nearly two-dimensional in the means; and (ii) a case in which vortex generators are used to induce a fixed array of longitudinal roll cells, allowing measurements to be made under stationary inflow and outflow regions. Burst frequencies obtained using an extension of the *uv*-quadrant method confirm the visual impression that inflows suppress the bursting process, while outflows enhance it. Reynolds-averaged measurements show that turbulence intensity and the *uv* correlation coefficient are also suppressed under the inflows. Based on these results, a conceptual model for the effects of large-scale eddies on near-wall flow and skin friction in a concave layer is proposed.

1. Introduction

This paper and a companion paper by Barlow & Johnston (1988, hereinafter referred to as I) on the overall effects of concave curvature on the structure of a turbulent boundary layer document a series of experiments in which detailed measurements were made in a flow where the behaviour of the large-scale, longitudinal roll cells produced by destabilizing curvature was thoroughly characterized through flow visualization. Results on the nature of these large-scale structures, as well as turbulence profiles across the full boundary layer, are included in I. The present paper focuses on the local effects of large-scale eddies on the near-wall flow and bursting process in the concave layer.

This investigation of the bursting process was motivated by an apparent contradiction between flow visualization results and time-averaged measurements. Dye visualization photographs from the present study, as well as previous visualization experiments by Jeans & Johnston (1982) and Simonich & Moffat (1982) in the same facility, have shown that the large-scale inflows and outflows that dominate the outer structure of the concave boundary layer have a much stronger

† Mechanical Engineering Department, Stanford University

influence on the near-wall flow than large eddies in a normal flat boundary layer. Conventional dye injection shows that sublayer streaks fan out under the inflows and converge under the outflows. The laser-induced fluorescence (LIF) photographs in I and in the present paper suggest that bursting is suppressed under the large-scale inflows, in that dye-marked fluid is rarely seen at any distance from the wall under the inflows. However, near-wall profiles of Reynolds-averaged turbulence quantities presented in I do not suggest any major change in structure. When the local value of the friction velocity, u_τ, is used for scaling, differences between the flat boundary layer and the natural concave boundary layer are limited to higher-order statistics, such as triple products, skewness, and flatness. (The following definitions are used throughout this paper: $y^+ = yu_\tau/\nu$, where y is distance normal to the wall, u_τ is the local friction velocity, and ν is the kinematic viscosity; $u^+ = \bar{U}/u_\tau$, where $\bar{U}$ is the mean streamwise velocity. Angle brackets, $\langle\ \rangle$, indicate the time average of a given turbulence quantity, and a prime indicates an r.m.s. value, i.e. $u' = \langle u^2 \rangle^{\frac{1}{2}}$ is the r.m.s. streamwise turbulence intensity.) The major terms associated with production of turbulence are not significantly altered inside $y^+ \approx 20$ by the new large-eddy structure in the concave flow. Furthermore, measurements of the instantaneous temperature distribution on the concave wall by Simonich & Moffat showed that the spanwise variation of the instantaneous Stanton number under the most energetic inflows did not exceed 15% of mean value. (Frequency response of the liquid-crystal walls was not high enough to resolve fully the Stanton number fluctuations due to small-scale, wall-layer structures, but was more than adequate to resolve the large-scale variations due to the inflows and outflows.) While interpretation of this result was complicated by the fact that the Prandtl number in this water flow was about 6, the effect of the large-scale motions near the wall, where most of the temperature difference exists, was less than the investigators had anticipated, based on the flow visualization.

Bursting is understood to be the principal process by which low-speed fluid from the viscous sublayer is mixed out to the rest of the boundary layer. It is important to the transport of thermal energy as well as momentum. Based on the results of the visualization studies, we formulated the hypothesis that the instantaneous effects of the large-scale motions were less than one might otherwise expect, because the bursting process was suppressed by the inflow and enhanced under the outflow, partially counteracting the effects of having local concentrations of high-momentum fluid (inflow) or low-momentum fluid (outflow) near the wall. Results included here show that this hypothesis is substantially correct.

The dominant coherent structure in the near-wall region of a turbulent shear flow is the array of alternating low-speed and high-speed streaks first observed by Kline & Runstadler (1959) and further documented by Schraub & Kline (1965), Kline *et al.* (1967), and Kim *et al.* (1971), and others. Following the terminology of Kim *et al.*, bursting refers to the entire process, by which a low-speed streak lifts up from the wall, oscillates, then breaks up into chaotic motion, ejecting low-momentum fluid out into the boundary layer. A related structure consisting of the movement of high-velocity fluid toward the wall was first observed by Corino & Brodkey (1969) and is generally described as a sweep. Those visualization studies showed that sweeps and ejections were major contributors to the production of turbulent shear stress and turbulent kinetic energy in wall-bounded flows. Subsequently, many experiments have been conducted to further investigate near-wall coherent structures, to quantify the contributions of these structures to time-averaged turbulence statistics, and to develop techniques for identifying 'burst' events with single-probe

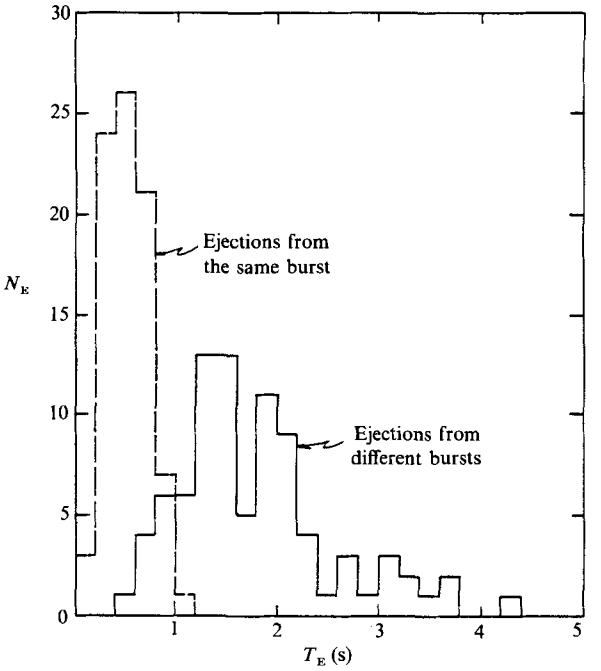

FIGURE 1. Histograms of times between ejections from the same burst and from different bursts (from Bogard 1982).

measurements. Reviews of much of this experimental work have been provided by Willmarth (1975, 1978), Kline (1978), Cantwell (1981), Smith (1984), and Luchik & Tiederman (1987). Additional insights have been provided by Kim and Moin through a series of numerical simulations on near-wall structure (Moin & Kim 1982; Kim 1983; Moin & Kim 1985; Kim & Moin 1985).

A variety of probe methods for burst detection have been proposed which search for characteristics of the velocity signals that are postulated to be associated with the bursting process. These methods have produced widely different values for the mean burst frequency or period, even when applied in the same flow, and, in general, the correlation between the detected events and the visually defined bursting process has been unclear. Offen & Kline (1975) investigated this situation using simultaneous flow visualization and probe measurements and concluded that there was inadequate correlation between the visual burst events and any of the detection schemes they considered.

Bogard & Tiederman (1986) conducted a similar combined visualization and probe study addressing the same issue. Experiments were carried out in a fully developed channel flow, using simultaneous hydrogen-bubble and dye flow visualization and a hot-film probe. Several single-probe, burst-detection methods were considered, and parameters for each method were optimized to maximize the probability of correct detections as defined by visual results, while maintaining a low probability of false detections. Probe methods are generally more repeatable for quantitative measurements than visual methods. However, for recognition of an event involving a coherent structure in the flow, there is little doubt that carefully applied visual methods are more 'accurate' than probe methods. Thus, the view taken by Bogard & Tiederman that visual results be used as a basis for evaluating probe methods is

seen as appropriate by the present authors. Bogard & Tiederman concluded that the uv-quadrant method gave the best correlation between probe detections and visually observed ejections.

Visual studies have shown that there can be more than one ejection in a single burst event, since fluid from the uplifting streak can be contorted into more than one outward-moving structure through the oscillation and breakup phases of the process. Offen & Kline identified about two ejections per burst, on average. Bogard & Tiederman found a similar result for the average number of ejections per burst, and figure 1 shows the histograms they obtained for the time, T_E, between visually observed ejections from the same burst and from different bursts. This possibility of multiple ejections must be accounted for if a probe method is to detect bursts in a manner consistent with the visually defined phenomenon. For the data in figure 1, a cutoff time, τ_E, of roughly 0.8 s could be used to group ejections into bursts without misidentifying many ejections. This observation was the basis for the burst-detection method developed by Bogard (1982), refined by Bogard & Tiederman (1986) and further modified in the present work.

In the following sections, the experimental techniques are outlined, the burst-detection method is described, local effects of the large-scale inflows and outflows on burst frequencies are quantified, and a conceptual flow model for the effects of curvature on wall-layer structure is proposed.

2. Experimental apparatus

Descriptions of the flow facility, the visualization techniques, and the laser-Doppler anemometry (LDA) system are included in I, with complete details given in Barlow & Johnston (1985). Briefly, experiments were carried out in a low-speed water channel, with a free-stream velocity of about 15 cm/s. A turbulent boundary layer was grown along the straight portion of the test wall to a thickness of about 7.5 cm at a momentum-thickness Reynolds number of roughly 1300. This layer then flowed through a 90° curve of constant radius, such that the curvature parameter, δ_0/R, was 0.055, with δ_0 being the boundary-layer thickness at the start of curvature and R being the wall radius. Dye slots were built into the test wall at several streamwise locations.

The LDA system was based on a TSI three-beam, two-component configuration, with the receiving optics oriented for 90° side-scatter. This orientation reduced the size of the measuring volume to a diameter of about 1.5 wall units and a length in the spanwise direction of about 3 wall units. These dimensions were comparable to the Kolmogorov lengthscale in the flow, which was estimated to be about 2 wall units. This estimate of the Kolmogorov scale is based on measured values of $\partial\bar{U}/\partial y$ and $-\langle uv\rangle$ near $y^+ = 15$ and the assumption that production equals dissipation in that region. Analog signals from two counters were sampled at fixed intervals. Data rates were typically well above any significant energy-containing frequencies, so that all important turbulence scales were resolved. This resolution is demonstrated by spectral data in I and in figure 8.

3. Use of vortex generators to lock the roll-cell pattern

The objective of this study was to obtain quantitative results on the local effects of the large-scale inflows and outflows on near-wall turbulence structure. Accordingly, two flow cases were investigated: (i) a natural, concave boundary layer in

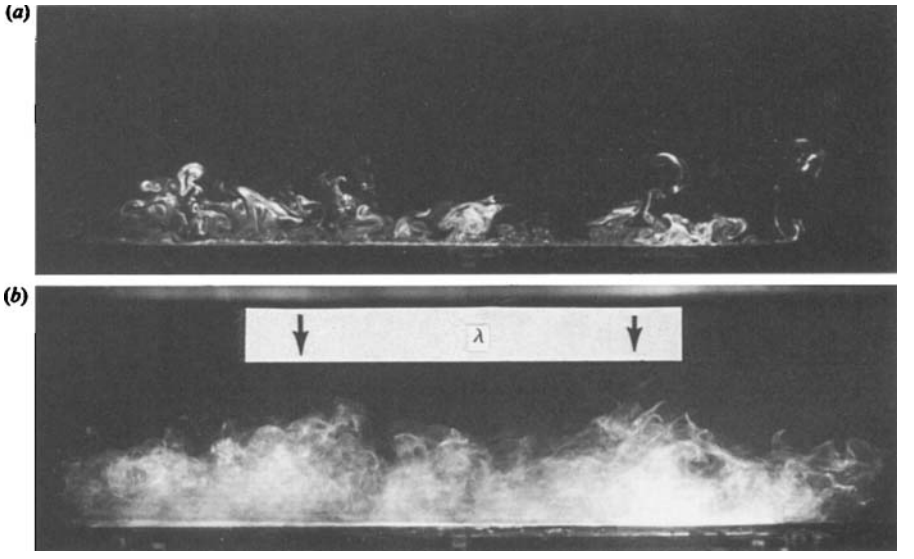

FIGURE 2. Laser-induced fluorescence photographs in the flat boundary layer with the 3.8 cm high, $\lambda = 15.2$ cm vortex generators. Dye injected 60 cm upstream of the laser sheet. (*a*) $\frac{1}{125}$ s exposure; (*b*) 2 s exposure.

which the large-scale inflow and outflow regions appeared randomly across the span, with the boundary layer remaining nearly two-dimensional in the mean (the case documented in I); and (ii) a case where vortex generators were placed at the beginning of the straight development section to produce a controlled disturbance that was amplified by destabilizing curvature to lock the large-scale roll cells into stationary spanwise locations. With the roll cells locked, burst frequencies and other turbulence quantities could be measured under the inflow and outflow regions separately, without the need for conditional sampling to detect the passing of these large-scale structures. (This use of vortex generators follows the work of Hoffmann, Muck & Bradshaw 1985.)

In the second flow case, arrays of half-delta-wing vortex generators were placed across the span of the test wall at the beginning of the straight development section, roughly 4.8 m upstream of the onset of curvature. The ratio of chord length to height was fixed at 4.0, and the vortex generators were set at alternating $+11°$ and $-11°$ angles to the flow. Generator height and wavelength were varied independently, and the resulting roll-cell pattern for each combination was visualized by conventional dye injection. Vortex generators with a height of 3.8 cm and a spanwise wavelength of 15.2 cm produced the most stable roll-cell pattern in the curve, while those with a height of 2.5 cm and a wavelength of 10.2 cm were the smallest vortex generators to produce an acceptably stable visual pattern. Laser-induced fluorescence (LIF) photographs, showing cross-sections in the (y, z)-plane of the flat and 60° boundary layers, are provided in figures 2 and 3 for the flow with the larger vortex generators. These photographs may be compared with corresponding images in the natural flow (I, figures 7, 8, 11 and 12). While the outflow locations in the flat boundary layer are faintly visible in figure 2(*b*), the embedded vortices had no visually detectable effect on the near-wall flow. These relatively weak vortices were amplified along the concave surface to produce the fixed pattern of roll cells shown in figure 9. Here, as in the natural flow, the influence of the large-scale roll cells on the near-wall flow was

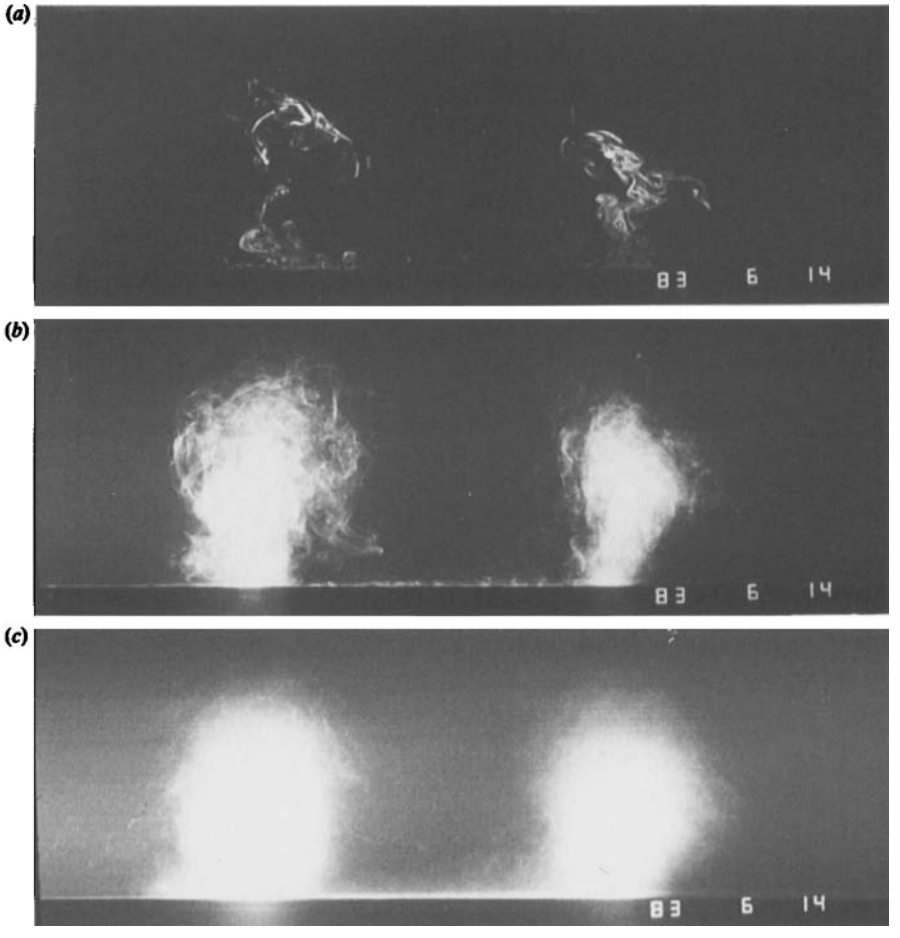

FIGURE 3. Laser-induced fluorescence photographs showing stationary outflows at 60° in the vortex-generator flow. Dye injected 60 cm upstream of the laser sheet. (*a*) $\frac{1}{125}$ s exposure; (*b*) 2 s exposure; (*c*) 60 s exposure.

significant. Dye-marked fluid rarely left the wall region under the inflows. Rather, the sublayer fluid was spread laterally and moved away from the wall at the bases of the large-scale outflows. The stability of the spanwise locations of the roll cells is demonstrated in the 60 s LIF exposure, figure 3(*c*). (Compare Paper I, figure 12.)

Velocity measurements (in Barlow & Johnston 1985) showed that the larger vortex generators produced a greater disturbance of the upstream boundary layer than was considered acceptable. Consequently, detailed turbulence measurements were made only in the flow with the smaller (2.5 cm) generators. Representative dye-visualization photographs in figure 4 show that the roll cells induced by these 2.5 cm vortex generators meandered slightly but remained continuous throughout the curve.

Spanwise surveys of mean velocity and streamwise turbulence intensity, taken at the flat and 60° stations in the flow with the 2.5 cm vortex generators, are plotted in figures 5 and 6, respectively. Outflows are marked by narrow valleys in $\bar{U}$ and broad peaks in u'. Conversely, inflows have broad peaks in $\bar{U}$ and narrow valleys in u'. The turbulence surveys reveal an important difference between the flat and concave

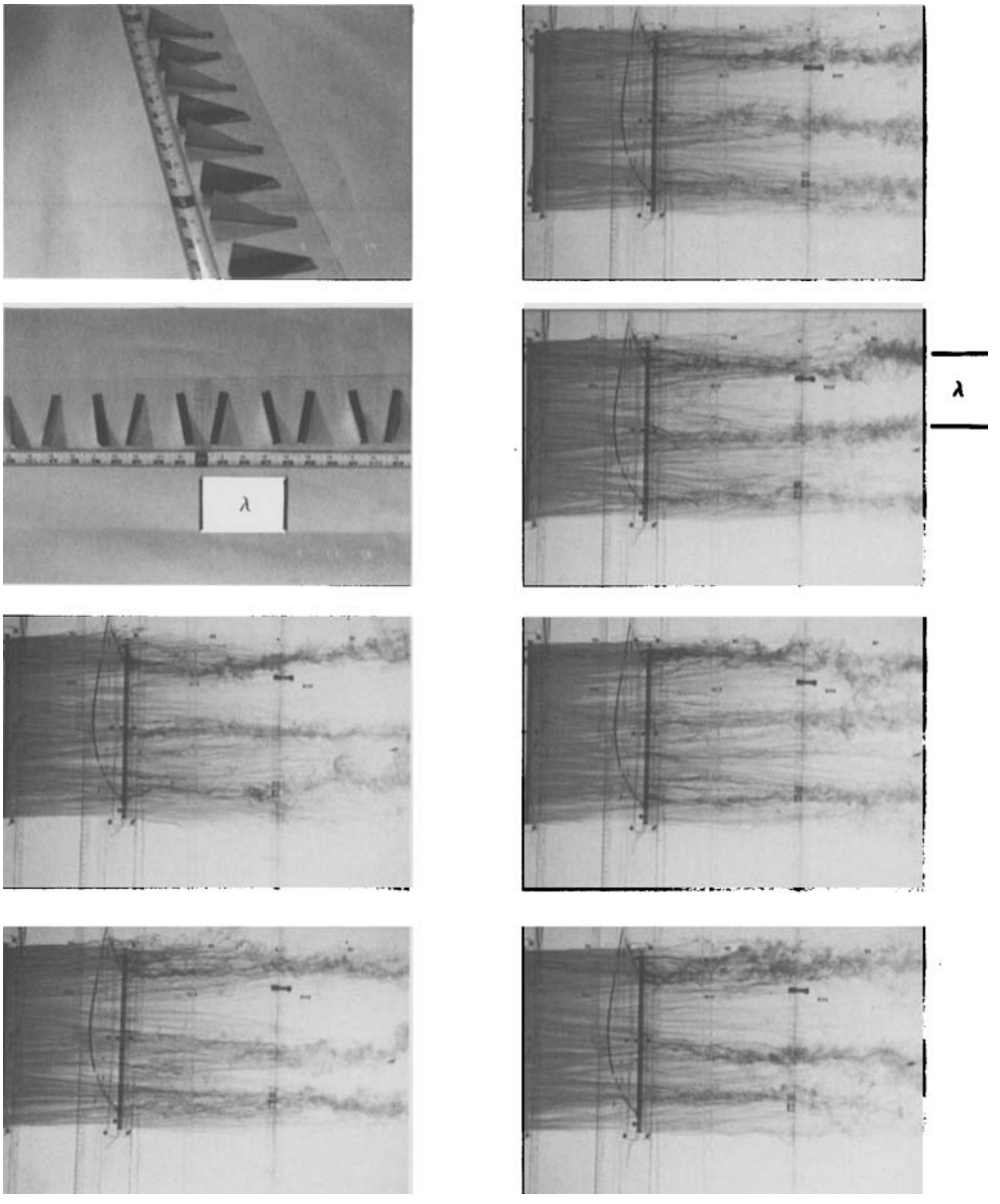

FIGURE 4. 2.5 cm high, $\lambda = 10.2$ cm vortex generators and resulting flow pattern in the curve. The dye-marked outflows meander but are continuous throughout the field of view (from 25° to 55° of turn).

cases. The data taken at $y = 1$ cm show little spanwise variation in u' (figure 5*b*). This suggests that the vortices ride along in the outer layer and do not strongly affect the flow near the wall. At the 60° station, however, there is significant spanwise variation in the survey of u' at $y = 1$ cm (figure 6*b*). Clearly, the roll cells in the curve penetrate farther toward the wall after being amplified by the Taylor–Görtler mechanism.

The spanwise wavelength (10.2 cm) of these induced roll cells was similar to the typical wavelength of roll cells in the natural flow. More importantly, the spanwise-

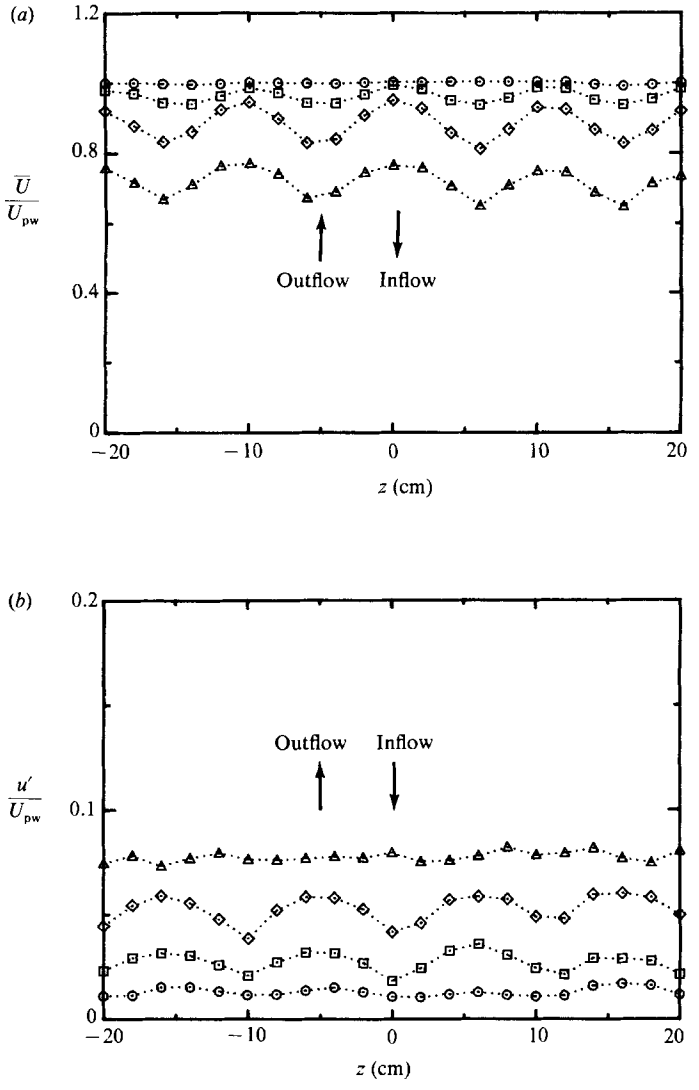

FIGURE 5. Spanwise surveys of (a) $\bar{U}/U_{pw}$ and (b) u'/U_{pw} at the flat station in the flow with 2.5 cm vortex generators: △, $y = 1$ cm; ◇, $y = 4$ cm; □, $y = 8$ cm; ○, $y = 12$ cm.

average skin-friction coefficient in the flow with vortex generators was only about 5% above that in the natural flow and followed the same trend in streamwise development, as shown in figure 7. This indicates that the main effect of the smaller vortex generators was to organize the flow at the largest scales, without significantly altering the underlying turbulence structure. This assessment is supported by figure 8, which compares spectra of velocity fluctuations normal to the wall at the 60° station for the two flow cases. Differences between the flat and concave cases are limited to the lowest frequency range of spectra at $y/\delta = 0.4$, the frequency range corresponding to the observed passing-frequency range of large-scale inflows and outflows in the natural concave boundary layer. Thus, we consider the roll cells in the

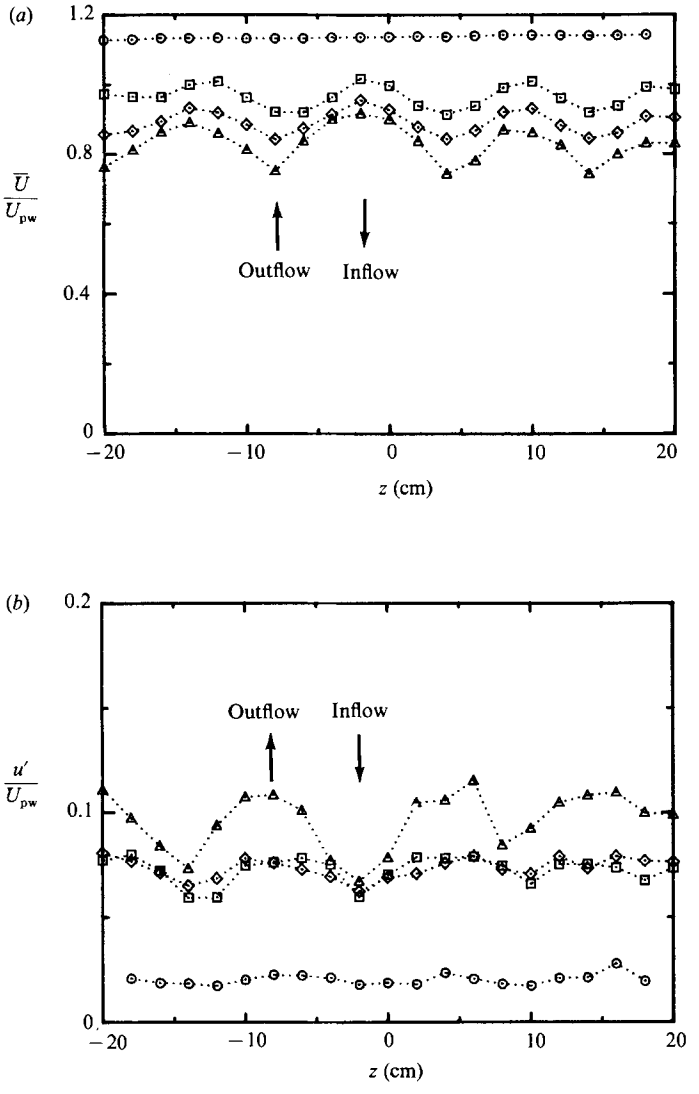

FIGURE 6. Spanwise surveys of (*a*) $\bar{U}/U_{pw}$ and (*b*) u'/U_{pw} at the 60° station in the flow with 2.5 cm vortex generators: △, $y = 1$ cm; ◇, $y = 4$ cm; □, $y = 8$ cm; ○, $y = 16$ cm.

flow with vortex generators to be representative of the more energetic roll cells in the natural flow, and we believe that measurements in the flow with vortex generators may be used to interpret the local effects of the inflows and outflows in the natural concave boundary layer on the bursting process and on turbulence levels near the wall.

Table 1 summarizes the boundary-layer parameters at the flat and 60° stations in the natural flow and at the centres of the induced inflow and outflow regions. The peak values of $\bar{V}$, the mean velocity normal to the wall, are included as a measure of the strength of the secondary flow pattern in the case with vortex generators. Curvature amplifies the peak $\bar{V}$ values by factors of three to four.

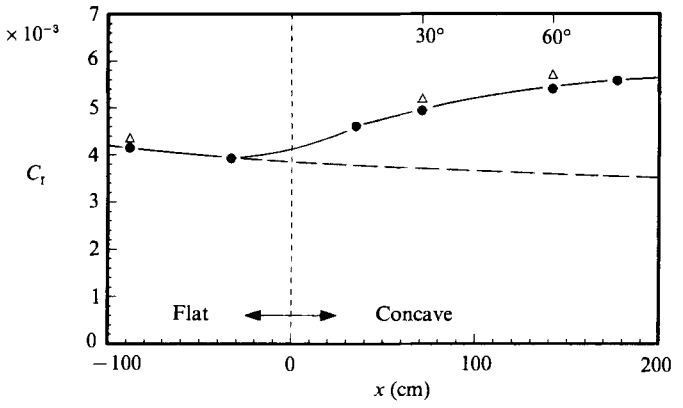

FIGURE 7. Streamwise development of the spanwise-average value of C_f: ●, natural flow; △, vortex generators. The dashed line represents the expected development in a flat boundary layer.

	Flat			60°		
	Natural	Inflow	Outflow	Natural	Inflow	Outflow
x (cm)	−88	−88	−88	142	142	142
U_{pw} (cm/s)	14.9	15.4	15.3	14.8	.4.8	14.9
u_τ (cm/s)	0.68	0.74	0.65	0.77	0.80	0.72
ν (cm²/s)	0.0099	0.0103	0.0103	0.0104	0.0095	0.0103
δ_{99} (cm)	6.4	7.4	11.1	12.1	13.2	13.9
δ_{99}/R	0.000	0.000	0.000	0.088	0.096	0.101
δ^* (cm)	1.10	0.91	1.83	1.45	0.92	2.05
θ (cm)	0.75	0.65	1.29	1.18	0.82	1.65
Re_θ	1140	970	1920	1680	1270	2390
H	1.46	1.41	1.42	1.23	1.13	1.24
G	6.87	6.07	7.05	3.58	1.92	4.03
C_f	0.0042	0.0046	0.0036	0.0054	0.0072	0.0046
$\bar{V}_{max}/\bar{U}_{pw}$	—	−0.008	0.016	—	−0.038	0.060

x Streamwise distance from the start of curvature.

U_{pw} Potential flow velocity extrapolated to the wall.

u_τ Friction velocity.

δ^*, θ Displacement thickness and momentum thickness as defined for curved flows by Honami & Johnston (1982).

$$\delta^* = R_{exp}\left[\frac{1}{U_{pw}R}\int_0^\delta (U_p - \bar{U})\,dy - 1\right], \quad \theta = R\left[(1 - \frac{1}{U_{pw}^2 R}\int_0^\delta \bar{U}(U_p - \bar{U})\,dy)^{-1} - 1\right],$$

where U_p is the potential flow velocity.

Re_θ Momentum thickness Reynolds number, $U_{pw}\theta/\nu$.

H Shape factor, δ^*/θ.

G Clauser shape factor, $(2/C_f)^{\frac{1}{2}}(H-1)/H$.

C_f Skin-friction coefficient. C_f and u_τ are determined by a log-law fit, with $\kappa = 0.41$ and $C = 5.0$, except for the 60° inflow case, where the velocity gradient in the sublayer is used to calculate wall shear. (See Barlow & Johnston 1985 for details.)

TABLE 1. Boundary-layer parameters

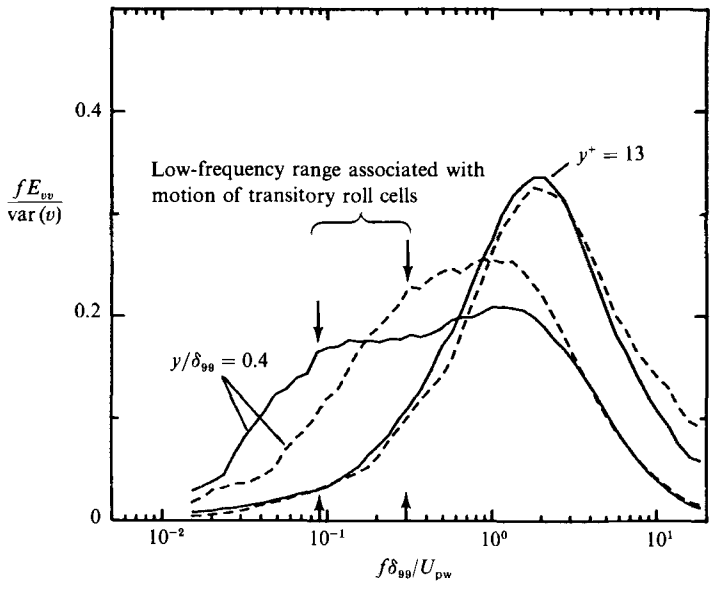

FIGURE 8. Effect of the vortex generators on v-spectra in the concave boundary layer at the 60° station: ——, natural flow; ——, centre of inflow.

4. The burst-detection method

Bogard & Tiederman (1986) proposed a burst-detection method that uses the uv-quadrant technique to identify ejections, then groups the ejections into bursts according to the probability distribution of times between ejections, $F[T_E]$. A cutoff time, τ_E is determined by comparing $F[T_E]$ to the theoretical probability distribution for random events having a fixed, finite duration. Any two ejections that occur within τ_E of each other are grouped into the same burst, but if the time between two ejections is greater than τ_E the second ejection is identified as the beginning of a new burst.

The method used in the present study is the same as that developed by Bogard & Tiederman, except that a different procedure is proposed of determining τ_E which appears to be more consistent with the physics. Probability distributions for times between ejections in the normal, flat boundary layer are plotted on semilog coordinates, as in figure 9. The experimental distribution, $1-F[T_E]$, is linear in these coordinates for values of the abscissa, $T_E/\bar{T}_E$, greater than about 1.0. Low values of T_E are assumed to be associated with ejections in the same burst, while high values of T_E are associated with ejections from different bursts. Clearly, the two groups follow different statistics. The cutoff time, τ_E, for separating ejections into these two groups is determined from the intersection of fitted lines, A and B, as shown in figure 9. Line A is drawn through the linear portion of the data and line B is drawn from the origin and tangent to the data. This procedure for defining the cutoff or grouping time, proposed by Barlow & Johnston (1985), has been adopted by Luchik & Tiederman (1987) and applied by them to several other single-probe burst-detection methods.

Figure 10 demonstrates how the resulting burst-detection method works. Sample records of the u, v, and uv fluctuations measured at $y^+ = 20$ in the normal flat boundary layer are shown. When u is negative and v is positive (quadrant 2) and the

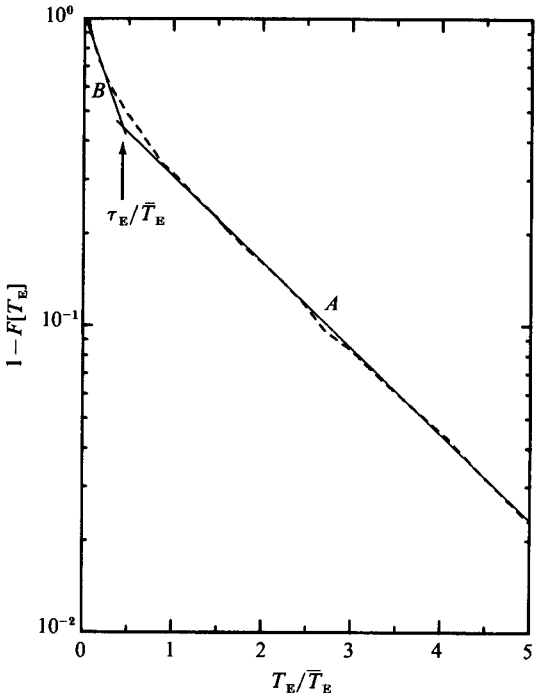

FIGURE 9. Graphical method of determining the cutoff time τ_E from the probability distribution of T_E. $\tau_E/\bar{T}_E$ is defined by the intersection of fitted lines A and B. Case of $y^+ = 20$, natural flow, flat station.

magnitude of uv is beyond the threshold, the event is tagged as an ejection at the time corresponding to the negative peak in uv. Following the recommendations of Comte-Bellot, Sabot & Saleh (1978) and Bogard & Tiederman (1986), the threshold is defined as $\langle uv_2 \rangle$, the conditionally averaged mean of uv in the second quadrant. If the time between a given ejection and the previous one is less than τ_E, the ejection is considered to be part of the burst that is in progress. When the time between successive ejections is greater than τ_E, the second ejection is tagged as the beginning of a new burst.

Note that u remains negative through the duration of the second and third 'bursts' in figure 10, in which several ejections have been grouped together. This suggests that each chain of ejections was correctly identified as being part of a single, larger structure. The last ejection in the second 'burst' is followed by a rapid increase in u. This event would be detected by the VITA technique of Blackwelder & Kaplan (1976), as would the rapid rise in u following the first 'burst' in figure 10, which consists of a single ejection. In fact, when the VITA threshold was adjusted to produce about the same total number of detections as the present method, a VITA detection followed the last ejection in a 'burst' by less than τ_E roughly two-thirds of the time, with the remaining VITA detections being essentially unassociated with ejections detected by the quadrant method. Unfortunately, due to time constraints, this comparison was not pursued further.

The probability distribution of times between ejections behaves essentially the same way in the concave boundary layer as in the flat boundary layer, i.e. the experimental curve is nearly linear for longer times. Thus, the method can also be applied to the concave boundary layer. Once the method has been applied, the

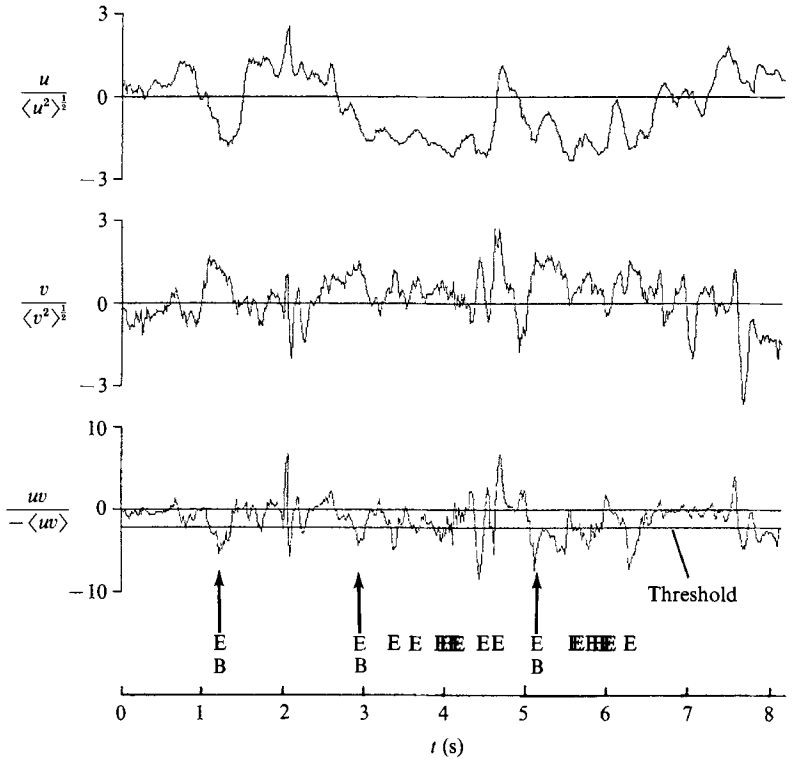

FIGURE 10. Sample data records at $y^+ = 20$ in the flat boundary layer showing how the burst-detection method works. Case of $y^+ = 20$, natural flow. The detection threshold for ejections is set equal to $\langle uv_2 \rangle$, the mean value of uv in quadrant 2. E = ejection; B = burst.

statistical behaviour of the bursts can be examined. This is done in figure 11, which shows a semilog plot of the conditional probability distribution of time between bursts, $1 - F[T_B | T_B > \tau_E]$. (By definition, of course, T_B cannot be less than τ_E but it is important to point out that this is a conditional probability distribution, so the origin on the abscissa does not correspond to zero time between bursts.) One finds that the detected bursts are exponentially distributed, and agreement with the theoretical distribution is particularly good for the flat boundary layer. Kim *et al.* (1971) and Bogard (1982) concluded from visual studies that the times between near-wall events had log-normal distributions. As seen in figure 1, the use of a fixed cutoff time results in the misidentification of some ejections, causing the differences in burst statistics in the range of shorter times. Except for this detail, the present method appears to be consistent with the physics of the bursting process as it is understood through visual studies.

The mean burst period obtained by this method at $y^+ = 20$ in the flat boundary layer without vortex generators was $\overline{T_B^+} \approx 80$, where $\overline{T_B^+} = \overline{T_B} u_\tau^2 / \nu$. This result is in good agreement with visualization studies of zero-pressure-gradient boundary layers (Kim *et al.* 1971; Kline *et al.* 1967). Luchik & Tiederman obtain a somewhat longer burst period ($T_B^+ \approx 90$). However, the uncertainty intervals for these two experiments overlap, and the latter result is also within the scatter of flow-visualization data.

Figure 12 shows the effects on $\overline{T_B^+}$ of varying the uv threshold and τ_E for the flat boundary layer. While $\overline{T_B^+}$ is not independent of threshold, it is relatively insensitive, such that more than doubling the threshold from 0.6 $\langle uv_2 \rangle$ to 1.4 $\langle uv_2 \rangle$ causes a

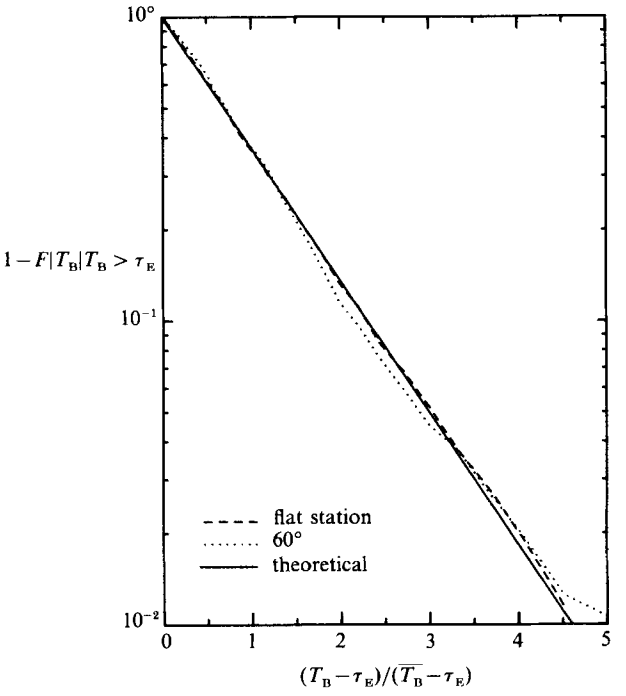

FIGURE 11. Probability distributions of times between bursts, T_B, for the flat and 60° boundary layers, at $y^+ = 20$ in the natural flow.

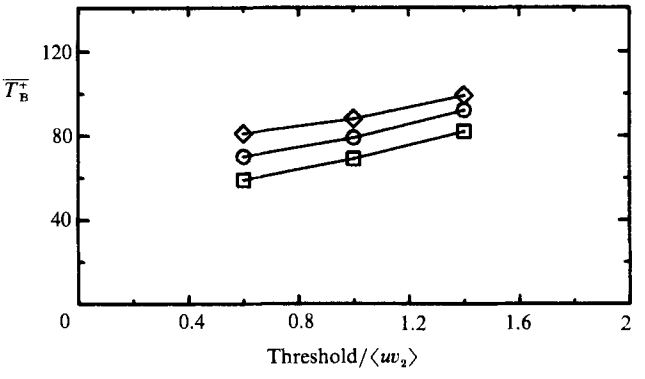

FIGURE 12. Sensitivity of $\overline{T_B^+}$ to variations of the detection threshold and τ_E at $y^+ = 20$ in the flat boundary layer: $\tau_E =$: □, 0.35 s; ○, 0.45 s; △, 0.55 s.

change in $\overline{T_B^+}$ of just 30 %. The method is more sensitive to changes in τ_E, but varying τ_E by ±22 % about the 'best' value only changes $\overline{T_B^+}$ by roughly ±13 % for the flat-boundary-layer data. This range of τ_E is representative of the uncertainty in $\overline{T_B^+}$ due to ambiguity in drawing the lines to determine τ_E.

4. Mean burst frequencies

Velocity-time records at $y^+ = 20$ were obtained at the flat and 60° stations in the natural flow and at the centres of the inflow and outflow regions in the flow with vortex generators. Boundary-layer parameters for these cases are listed in table 1.

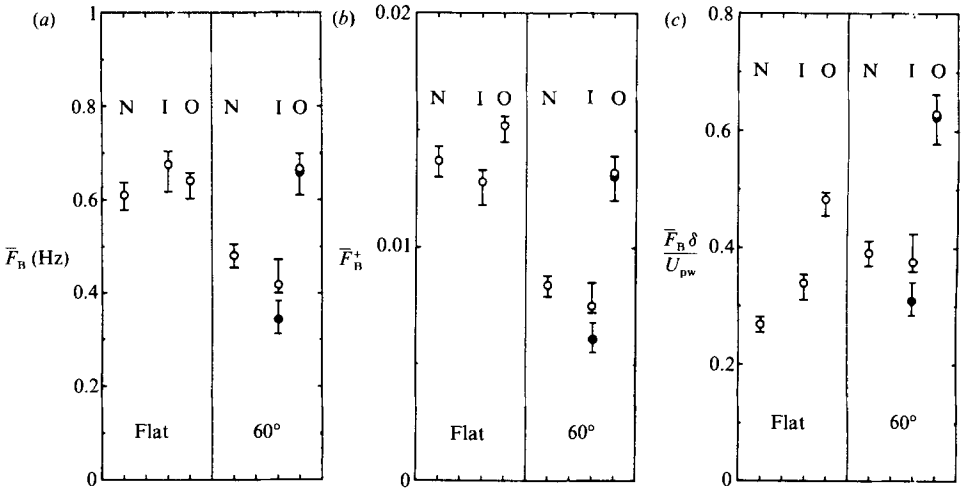

FIGURE 13. Mean burst frequencies at $y^+ = 20$ in the flat and 60° boundary layers using: (*a*) no scaling; (*b*) inner scaling; (*c*) outer scaling. Threshold = : ○, $\langle uv_2 \rangle_{local}$; ●, $1.05\langle uv_2 \rangle_{natural}$. N, I, and O denote natural flow, inflow, and outflow, respectively.

Ejections were detected and grouped into bursts according to the method described above, with records generally including over 3000 ejections. Resulting burst frequencies are plotted in figure 13. Blackwelder & Haritonidis (1983) and Luchik & Tiederman (1987) concluded that burst frequencies scale on inner variables. However, flow visualization has indicated a greater influence of large-scale eddies on near-wall structure in the concave boundary layer than in the flat boundary layer. The bursting process may result from interactions between sublayer structures and outer-layer eddies, and if this is the case, neither inner nor outer scaling could be expected to work well in all flows. Accordingly, burst frequencies are presented with inner scaling ($\bar{F}_B \nu/u_\tau^2$) and outer scaling ($\bar{F}_B \delta/u_{pw}$) as well as in raw form. The error boxes in figure 13 represent the range of frequencies corresponding to the range of values of τ_E that could be used for each data record due to ambiguity in drawing lines, such as those in figure 9.

A complete evaluation of the scaling of burst frequencies in curved flows would require data over ranges of Reynolds number and δ/R, and such data are not available. However, there is some indication in the present data that the outer flow has a significant influence on burst frequency. In the natural boundary layer, u_τ^2/ν is about 22% higher at the 60° station than at the flat station. Thus, if inner scaling were globally correct, one would expect the raw burst frequency at 60° of turn to be 22% higher than the raw frequency at the flat station. The measured burst frequency at 60° is 0.48 Hz, 21% lower than the 0.61 Hz frequency at the flat station. On the other hand, U_{pw}/δ in the natural flow case decreases by nearly a factor of two between the flat and concave stations, due to growth in boundary-layer thickness. If pure outer scaling were correct, one would expect a halving of the raw burst frequency. These results imply that the bursting process in the natural, concave boundary layer is influenced by both inner and outer flow parameters.

Turning to the flow with vortex generators, we find that the raw burst frequencies at the flat station are roughly the same for the natural, inflow, and outflow cases. Differences remain relatively small when inner scaling is applied (figure 13*b*), but there is some indication that bursting is suppressed under the inflow and enhanced

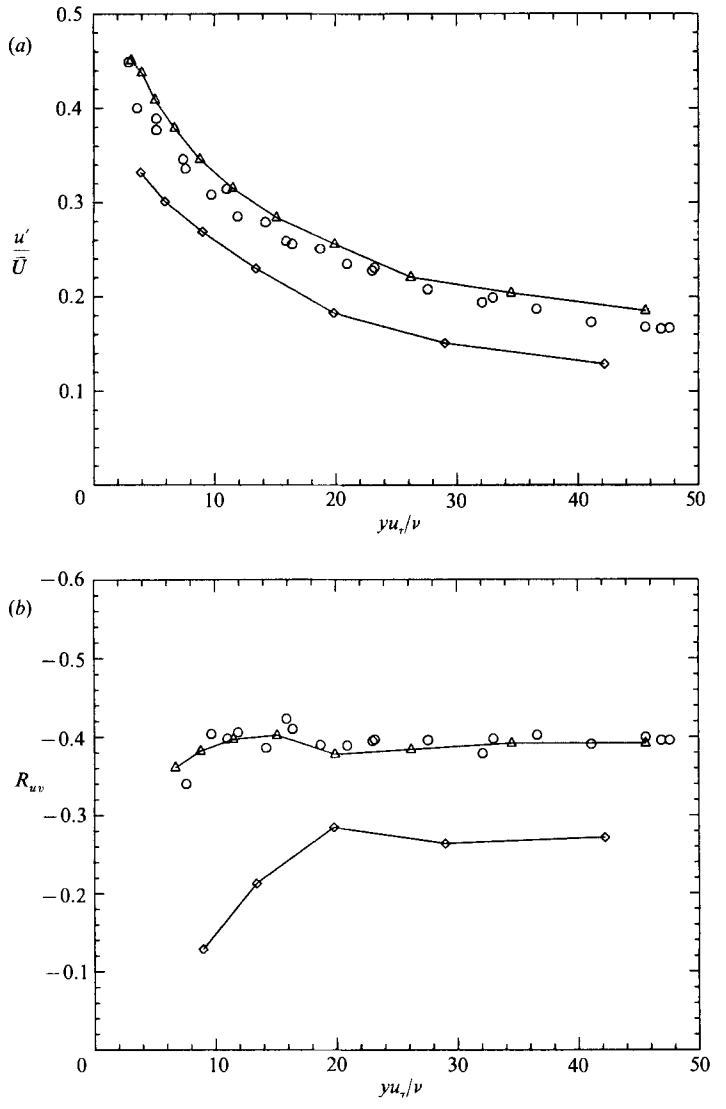

FIGURE 14. Near-wall profiles of (*a*) $u'/\bar{U}$ and (*b*) R_{uv} at the 60° station: ○, natural flow; ◇, inflow; △, outflow.

under the outflow relative to changes in u_τ. When outer scaling is used (figure 13*c*), the dimensionless burst frequency for the outflow is roughly 80% higher than for the natural flow. This is caused by the large local value of δ_{99}, and outer scaling appears to be inappropriate for this case, since the visualization results showed no significant effect of the vortex generators on the near-wall structure.

At the 60° station in the concave boundary layer, the problem of scaling is less important, since all three graphs in figure 13 show similar relationships between burst frequencies for the natural, inflow, and outflow cases. When the detection threshold is set to the local value of $\langle uv_2 \rangle$ (open symbols), the burst frequency for the inflow is slightly less than that for the natural flow, while the burst frequency for the outflow is significantly higher (60–75% higher, depending on which scaling is used). While this difference between outflow and inflow is consistent with visualization

results, it is much less dramatic. The burst-detection method, as applied here, indicates that there is still a significant amount of bursting under the inflows, whereas the LIF visualization showed that dye from the sublayer almost never reached the middle or outer parts of the boundary layer in the inflow regions, suggesting that the bursting process was all but shut off by the large-scale inflows. However, figure 14 shows that turbulence intensities, as well as the correlation coefficient, R_{uv}, were lower under the inflow. Consequently, the local value of $\langle uv_2 \rangle$, the detection threshold, was nearly 50% lower for the inflow than for the outflow, and an ejection could be that much weaker under the inflow and still be detected.

To compare inflows and outflows at a given streamwise station, it is more appropriate to use a single value for the detection threshold. The closed symbols in figure 13 represent burst frequencies for the inflow and outflow cases at the 60° station determined with the detection threshold set equal to 1.05 times the value of $\langle uv_2 \rangle$ in the natural flow at 60°. (The factor of 1.05 comes from the fact that the spanwise average value of C_f was about 5% higher in the flow with vortex generators.) This redefinition of the detection threshold causes only a small difference for the outflow. However, the detected burst frequency under the inflow is significantly reduced, with the resulting difference between outflow and inflow being roughly a factor of two, independent of scaling.

6. Discussion and conclusions

This paper has examined the local effects of large-scale inflows and outflows on the bursting process in a concave boundary layer by considering a flow where vortex generators were placed in the developing boundary layer upstream of the start of curvature. This paper has also presented a modification of Bogard & Tiederman's (1986) *uv*-quadrant burst-detection method.

As discussed in §2, the main effect of the vortex generators is to organize the large-scale roll cells into a stationary pattern, without changing significantly the structure of the intermediate and smaller turbulence scales or the spanwise-averaged skin friction. Thus, the results from the vortex generator case may be used in formulating a general, conceptual flow model for the effects of large-scale eddies on the wall region in concave boundary layers.

Under the inflows, high-momentum fluid from the outer part of the boundary layer impinges on the sublayer, thinning it locally. As a result, the short-time-average value of $\partial U/\partial y$ increases, and one would expect this to cause a significant increase in viscous shear. However, the inflow also causes suppression of turbulence in the wall region, as well as suppression of bursting. This tends to counteract, in part, the first effect, resulting in a more moderate local increase in wall shear than one might expect. Much of the fluid that leaves the sublayer under an inflow does so by being spread laterally toward neighbouring outflow regions, rather than being ejected directly into the outer boundary layer. Low-momentum fluid collects at the base of an outflow, thickening the sublayer, and one would expect this to decrease $\partial U/\partial y$ and thus decrease the local skin friction. However, turbulence levels and bursting are enhanced under the outflows, producing a compensating effect which tends to increase skin friction. On the whole, the difference in local wall shear between the inflow and outflow regions is less than one might have expected, given the very strong influence of these large-scale eddies on the visualized structure of the near-wall region. This model is consistent with the result from I that the r.m.s. fluctuation of wall shear is no greater, relative to the mean shear, in the natural, concave

boundary layer than in the normal flat boundary layer. This physical model also resolves the apparent conflict between previous results of Jeans & Johnston and Simonich & Moffat regarding the local effects of the large-scale motions in the concave boundary layer.

An implication of these results toward modelling of engineering flows, where prediction of skin friction or heat transfer is of primary concern, is that three-dimensional resolution of individual large structures by, say, large-eddy simulation should not be necessary, as long as the spanwise-average development of the boundary layer is predicted correctly. However, useful predictions will require that a turbulence model accurately account for the slow development of large-scale structure in concave flows described in the companion paper, Barlow & Johnston (1988).

This work was supported by the Air Force Office of Scientific Research. The authors are grateful to S. Kline, R. Moffat, P. Moin, J. Kim, D. Bogard, and W. Tiederman for many useful discussions during the course of this research.

REFERENCES

Barlow, R. S. & Johnston, J. P. 1985 Structure of turbulent boundary layers on a concave surface. *Rept. MD*-47, Thermosciences Div., Dept. of Mech. Engng. Stanford University.

Barlow, R. S. & Johnston, J. P. 1988 Structure of a turbulent boundary layer on a concave surface. *J. Fluid Mech.* **191**, 137.

Blackwelder, R. F. & Kaplan, R. E. 1976 On the wall structure of the turbulent boundary layer. *J. Fluid Mech.* **76**, 89.

Blackwelder, R. F. & Haritonidis, J. H. 1983 Scaling of burst frequencies in turbulent boundary layers. *J. Fluid Mech.* **132**, 87.

Bogard, D. G. 1982 Investigation of burst structures in turbulent channel flows through simultaneous flow visualization and velocity measurements. PhD dissertation, Purdue University.

Bogard, D. G. & Tiederman, W. G. 1986 Burst detection with single-point velocity measurements. *J. Fluid Mech.* **162**, 389.

Cantwell, B. J. 1981 Organized motion in turbulent flow. *Ann. Rev. Fluid Mech.* **13**, 457.

Comte-Bellot, G., Sabot, J. & Saleh, I. 1978 Detection of intermittent events maintaining Reynolds stress. *Proc. Dynamic Flow Conf. Dynamic Measurements in Unsteady Flows*, p. 213. Marseille.

Corino, E. R. & Brodkey, R. S. 1969 A visual study of turbulent shear flow. *J. Fluid Mech.* **65**, 1.

Hoffmann, P. H., Muck, K. C. & Bradshaw, P. 1985 The effect of concave curvature on turbulent boundary layers. *J. Fluid Mech.* **161**, 371.

Jeans, A. H. & Johnston, J. P. 1982 The effects of concave curvature on turbulent boundary-layer structure. *Rept. MD*-40, Thermosciences Div., Dept. of Mech. Engng. Stanford University.

Kim, J. 1983 On the structure of wall-bounded turbulent flows. *Phys. Fluids* **26**, 52.

Kim, H. T., Kline, S. J. & Reynolds, W. C. 1971 The production of turbulence near a smooth wall in a turbulent boundary layer. *J. Fluid Mech.* **50**, 133.

Kim, J. & Moin, P. 1985 The structure of the vorticity field in turbulent channel flow. *J. Fluid Mech.* **162**, 339.

Kim, J., Moin, P. & Moser, R. 1987 Turbulence statistics in fully developed channel flow at low Reynolds number. Submitted to *J. Fluid Mech.*

Kline, S. J. 1978 The role of visualization in the study of the structure of the turbulent boundary layer. In *Coherent Structure of Turbulent Boundary Layers* (ed. C. R. Smith & D. E. Abbott). AFOSR/Lehigh University Workshop.

KLINE, S. J., REYNOLDS, W. C., SCHRAUB, F. A. & RUNSTADLER, P. W. 1967 The structure of turbulent boundary layers. *J. Fluid Mech.* **30**, 741.

KLINE, S. J. & RUNSTADLER, P. W. 1959 Some preliminary results of visual studies of the wall layers of the turbulent boundary layer. *Trans. ASME* E: *J. Appl. Mech.* **81**, 166.

LUCHIK, T. S. & TIEDERMAN, W. C. 1987 Timescale and structure of ejections and bursts in turbulent channel flow. *J. Fluid Mech.* **174**, 529.

MOIN, P. & KIM, J. 1982 Numerical investigation of turbulent channel flow. *J. Fluid Mech.* **118**, 341.

MOIN, P. & KIM, J. 1985 The structure of the vorticity field in turbulent channel flow. Part 1. Analysis of instantaneous fields and statistical correlations. *J. Fluid Mech.* **155**, 441.

OFFEN, G. R. & KLINE, S. J. 1975 A comparison and analysis of detection methods for the measurement of production in a boundary layer. *Proc. 3rd Biennial Symposium on Turbulence in Liquids*, Dept Chem. Engng, Univ. of Missouri, Rolla, p. 289.

SCHRAUB, F. A. & KLINE, S. J. 1965 A study of the structure of the turbulent boundary layer with and without longitudinal pressure gradients. *Rept MD*-12, Thermosciences Div., Dept Mech. Engng, Stanford University.

SIMONICH, J. C. & MOFFAT, R. J. 1982 Local measurements of turbulent boundary-layer heat transfer on a concave surface using liquid crystals. *Rep. HMT*-35, Thermosciences Div., Dept Mech. Engng, Stanford University.

SMITH, C. R. 1984 A synthesized model of the near-wall behavior in turbulent boundary layers. *Proc. Eighth Symposium on Turbulence* (ed. G. K. Patterson & J. L. Zakin), Dept Chem. Engng, University of Missouri-Rolla.

WILLMARTH, W. W. 1975 *Adv. Appl. Mech.* 15, 159.

WILLMARTH, W. W. 1978 Survey of multiple sensor measurements and correlations in boundary layers. In *Coherent Structure of Turbulent Boundary Layers* (ed. C. R. Smith & D. E. Abbott), AFOSR/Lehigh University Workshop.